AFRL-SN-HS-TR-2006-002

LONG LIFE MEM SWITCH TECHNOLOGY

Gabriel M. Rebeiz

University of Michigan
1058 Wolverine Tower - DRDA
Ann Arbor MI 48109-1274

23 May 2006

Final Report

AIR FORCE RESEARCH LABORATORY
Sensors Directorate
Electromagnetics Technology Division
80 Scott Drive
Hanscom AFB MA 01731-2909

TECHNICAL REPORT

Title: Long Life MEM Switch Technology

Unlimited, Statement A

NOTICE

USING GOVERNMENT DRAWINGS, SPECIFICATIONS, OR OTHER DATA INCLUDED IN THIS DOCUMENT FOR ANY PURPOSE OTHER THAN GOVERNMENT PROCUREMENT DOES NOT IN ANY WAY OBLIGATE THE US GOVERNMENT. THE FACT THAT THE GOVERNMENT FORMULATED OR SUPPLIED THE DRAWINGS, SPECIFICATIONS, OR OTHER DATA DOES NOT LICENSE THE HOLDER OR ANY OTHER PERSON OR CORPORATION; OR CONVEY ANY RIGHTS OR PERMISSION TO MANUFACTURE, USE, OR SELL ANY PATENTED INVENTION THAT MAY RELATE TO THEM.

THIS TECHNICAL REPORT HAS BEEN REVIEWED AND IS APPROVED FOR PUBLICATION.

_____//signature//_____
RICHARD T. WEBSTER
Program Manager

_____//signature//_____
LIVIO D. POLES
Chief, Antenna Technology Branch

_____//signature//_____
MICHAEL N. ALEXANDER
Technical Advisor
Electromagnetics Technology Division

REPORT DOCUMENTATION PAGE

Form Approved
OMB No. 0704-0188

1. REPORT DATE *(DD-MM-YYYY)*	**2. REPORT TYPE**	**3. DATES COVERED** *(From - To)*
31-03-2006	FINAL REPORT	15-SEP-2004 – 31-MAR-2006

4. TITLE AND SUBTITLE

Long Life MEM Switch Technology

5a. CONTRACT NUMBER
FA8718-04-C-0029

5b. GRANT NUMBER

5c. PROGRAM ELEMENT NUMBER
62204F

6. AUTHOR(S)

Gabriel M. Rebeiz

5d. PROJECT NUMBER
4916

5e. TASK NUMBER
HA

5f. WORK UNIT NUMBER
04

7. PERFORMING ORGANIZATION NAME(S) AND ADDRESS(ES)
University of Michigan
1058 Wolverine Tower - DRDA
Ann Arbor MI 48109-1274

8. PERFORMING ORGANIZATION REPORT NUMBER

9. SPONSORING / MONITORING AGENCY NAME(S) AND ADDRESS(ES)
Electromagnetics Technology Division
Sensors Directorate
Air Force Research Laboratory
80 Scott Drive
Hanscom AFB MA 01731-2909

10. SPONSOR/MONITOR'S ACRONYM(S)
AFRL/SNHA

11. SPONSOR/MONITOR'S REPORT NUMBER(S)
AFRL-SN-HS-TR-2006-002

12. DISTRIBUTION / AVAILABILITY STATEMENT
DISTRIBUTION A. Approved for public release; distribution unlimited.

13. SUPPLEMENTARY NOTES
Public Release number ESC 06-0588, 17 May 2006

14. ABSTRACT
Report developed under contract FA8718-04-C-0029. Microelectromechanical (MEM) switches have already been developed that demonstrate exceptional RF performance but have been plagued by poor reliability. In this work, two new MEM switches were developed with the goal of increasing reliability. The first is a miniature switched capacitor that is 150-300 times smaller than typical RF MEMS switches. The bridges on these switches are 21 micrometers long by 8 micrometers wide and have a switching time of less than 250 ns. Reliability of over 20 billion cycles of 0.5 W of RF power at 13 GHz was demonstrated. The second design is a switched capacitor that is a cantilever type of device. The switch showed a Q of more than 250 at X to Ku-band frequencies, and a reliability of more than 11 billion cycles at 1 W of RF power at 8 GHz. Finally, a tunable filter covering 5.1 and 5.7 GHz (two states) was designed, fabricated and tested. The loss was 1.4 dB, the bandwidth was 5%, and the tunable Q was over 150. These novel designs will be very useful for high reliability RF MEM switches and circuits in the coming years for commercial and defense applications.

15. SUBJECT TERMS
MEMS, switches, tunable filters, microwave components

16. SECURITY CLASSIFICATION OF:			**17.LIMITATION OF ABSTRACT**	**18.NUMBER OF PAGES**	**19a. NAME OF RESPONSIBLE PERSON**
a. REPORT	**b. ABSTRACT**	**c.THIS PAGE**			Eric Marsh
Unclassified	Unclassified	Unclassified	UU	26	**19b. TELEPHONE NUMBER** *(include area code)* --

Standard Form 298 (Rev. 8-98)
Prescribed by ANSI Std. Z39.18

Contents

1. Introduction

RF MEM switches and switched capacitors have been developed since 1997 for 4-120 GHz phase shifters, tunable filters and reconfigurable networks. These devices have shown outstanding performance in terms of insertion loss, isolation, intermodulation, and power consumption, and they have the potential to be very low cost. However they have some problems including speed, actuation voltage, power handling, and reliability. The objectives of this work are to develop very fast and high-reliability RF MEMS switched capacitors for use in X-band phase shifters and reconfigurable networks, and to use the high-reliability switches in the development of a high-Q switchable or tunable filter at 3-6 GHz.

2. Methods, Results, and Discussion

Two types of MEM switches were developed, and tunable filters based on MEM switches were then developed. This work has resulted in one published conference paper on the miniature switched capacitors, one paper on the cantilever switched capacitors that has been accepted to a conference as of this writing, and one journal paper on tunable filters that is in draft form. These three papers are included in the appendixes to this report, and they provide full background, design, results, and discussion on the work that was completed as part of this program.

2.1. MEM Switched Capacitors

The first type of MEM switch developed was the miniature switched capacitor. This device is 150-300 times smaller than conventional MEM switches such as the Raytheon switch. We fabricated the miniature capacitors again and tested them under high power conditions. The miniature capacitors (4x4 array) were tested at 13 GHz at 0.5-1 W and for 20 billion cycles and with no failures, hot switched. We also fabricated them in a 2-pole filter and measured the intermodulation distortion below -65 dBc at a carrier frequency of 17 GHz. This very low distortion translates to an third order intercept point of greater than 70 dBm, which is amazing! We have designed and successfully fabricated miniature RF MEMS devices and placed them in arrays (3x20) to increase their capacitance values. To fabricate these devices, we have modified the standard RF MEMS switch fabrication process. The pull-down voltage was 25 V and the measured switching speed was 250 ns. We did hot power measurements on them at 100 mW and have taken them to 20 billion cycles with no failures. The measured Q was greater than 150 at 10-20 GHz in the up-state position and greater than 100 in the down-state position.

We have also built a novel switched capacitor, based on the cantilever design, with a measured Q of greater than 300 at X-band frequencies and a capacitance ratio of 2.0. This switched-capacitor was tested at 1 W, hot switched, for 12 billion cycles at 8 GHz, with no failures. The switching time was measured to be 8 μs.

In-depth description and discussion of the miniature switched capacitors can be found in Appendix A, and for the cantilever device further discussion can be found in Appendix B.

2.2. Tunable Filters

We designed, fabricated, and tested a tunable filter covering 3 and 6 GHz (two states). The design was done on a quartz substrate with high Q resonators (Q=150) and was based on two concentric resonators (no via holes needed). This particular design employed standard RF MEMS switched capacitors since the main point was to see if we can switch a high Q resonator and we concentrated on the electromagnetic aspects of the problem, not on the RF MEMS aspects. Two different filters were designed: a fixed filter at 3.6 GHz and a tunable one covering 3 and 6 GHz. The fixed filter worked perfectly, with excellent agreement between theory and experiment and a measured Q greater than 150 (4% bandwidth and 1.8 dB insertion loss for a 2-pole filter). The tunable filter worked from 5.1 to 5.7 GHz since one of the switches failed to actuate, so we did not get the 3/6 GHz tuning. Still the loss was incredibly low, 1.3/1.4 dB, respectively for a 5% filter. The loss increased to 1.6/1.7 dB when no cover was used, showing the importance of shielding in high-Q filters. The tunable Q is greater than 150 which is 3-4 times improvement over earlier designs (tunable Q of 40-50).

Full technical detail on the tunable filter work can be found in Appendix C.

3. Conclusions and Recommendations

In this program, we have demonstrated for the first time RF MEMS switches which operate at around 200 ns switching time and have very high reliability even when tested at 0.5-1 W of RF power. We have also shown, again for the first time, a tunable and planar RF MEMS filter with a Q of 150, which is a record for an all-planar filter under any technology.

There is still a lot to be done: One of the main problems with capacitive RF MEMS is dielectric charging, and while the miniature MEMS switches did show a vast improvement over previous designs, they are still far from being impervious to this phenomena. We recommend more research effort in this area. Also, the packaging of the miniature MEMS switches was not done, and we also recommend that an in-situ dielectric-cap program be supported. Finally, the area of planar tunable filters is in its infancy, and we recommend that a large program on tunable filters covering 10 MHz to 18 GHz be funded.

APPENDIX A
Miniature RF MEMS Switched Capacitors

Denis Mercier, Koen Van Caekenberghe, and Gabriel M. Rebeiz

Electrical Engineering and Computer Science, The University of Michigan, Ann Arbor, MI, 48105, USA

***Abstract* — This paper presents a paradigm shift in RF MEMS, and shows the development of miniature switched capacitors for RF applications. The MEMS bridges are 21 µm long by 8 µm wide, and are 150-300× smaller than the standard Raytheon switch or other switched capacitors [1]. The bridges are integrated in an NxM array implemented in coplanar waveguide t-lines (CPW). The bridges are 3400 Å thick, and are suspended 2400 Å above the CPW center conductor (with a 1600 Å SiN layer), resulting in an actuation voltage of 25 V. The measured capacitance ratio of a single bridge is 2.8, and that of a 3x20 array is 1.9. These MEMS switched capacitors have a very high spring constant, and correspondingly a very high pull-up force per unit contact area with the dielectric layer. They are not sensitive to charging in the dielectric layer and also, are not sensitive to temperature variation. Also, the simulated switching time is 250 ns for gold switches and 110 ns for Al switches. We believe that this novel design will be very useful for high reliability RF MEMS switches in the coming years.**

***Index Terms* — RF MEMS, capacitors, reliability, switching speed.**

I. Introduction

RF MEMS switches and switched capacitors have been developed since 1997 for 4-120 GHz phase shifters, tunable filters and reconfigurable networks [1]. There are two different devices based on the capacitive approach: An RF MEMS switch with a capacitance ratio of 30-150, and an RF MEMS switched capacitor with a capacitance ratio of 2-6. The most common implementation of switched capacitors is using a standard RF MEMS switch in series with a fixed metal-insulator-metal (or metal-air-metal) capacitors. The RF MEMS switch is commonly used for routing purposes (SPNT, DPDT, NxN matrices), and switched-line phase shifter designs, while the switched capacitor is mostly used in tunable filters and reconfigurable networks.

It was shown that many phase shifter designs, such as the distributed MEMS t-lines or loaded-lines, require a capacitance ratio of 2.0 [1]. Also, tunable filters are generally implemented with a capacitance ratio of 2-2.5 since the tuning range is limited by the inverter design and not by the tunable resonators. The goal of this research is therefore to create a device with a capacitance ratio of 2-6 and with the potential of very high speed operation (50-250 ns), very high reliability even under dielectric charging conditions, reasonable operating voltages, and which can be easily packaged under high temperatures. As will be shown in this work, we believe that these can be all attained using the novel miniature RF MEMS switched- capacitor approach.

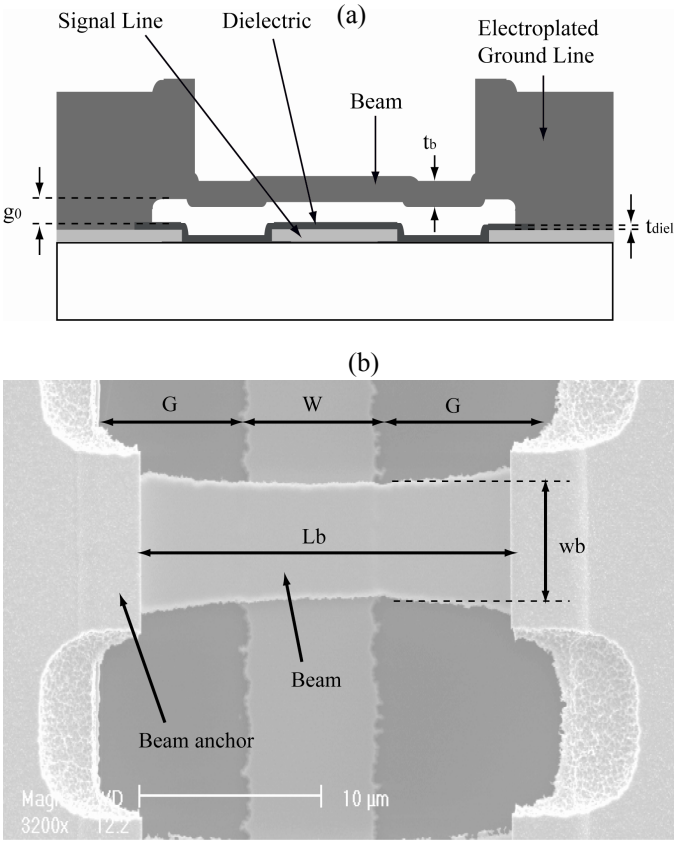

Fig. 1. Cross section of a miniature switched capacitor (a); SEM picture a miniature switched capacitor (b).

II. Structure

A cross section and a SEM top view of the fabricated structure are presented in Figs. 1. The structure is a shunt capacitive air-bridge, and when a voltage is applied between the signal line and the beam, the beam is pulled down and the shunt capacitance to the ground is increased.

The mechanical behavior of the MEM capacitor is designed using conventional mechanical equations detailed in [1] and has been checked with the finite element method CoventoreWare3 [2]. The dimensions of the fabricated structures are given in Table I. The spring constant k=70 N/m is calculated using (1), where E is the Young modulus in Pa, σ is the residual stress in Pa and υ is the Poisson coefficient:

$$k = k1 + k2 = \frac{32Ew_b t_b^3}{L_b^3\left[2-\left(2-\frac{W}{L_b}\right)\left(\frac{W}{L_b}\right)^2\right]} + \frac{8\sigma(1-\upsilon)w_b t_b}{L_b\left(2-\frac{W}{L_b}\right)} \quad (1)$$

A closer look at (1) shows that the value of k2, which is the residual stress component of the spring constant, is about 30% of k, while it is about to 80-90% in most reported capacitive switches. And, therefore, the switch pull-down voltage is much less sensitive to the residual stress in the beam, which can change significantly with temperature [3]. This is shown in Fig. 2 for the miniature switch with a residual stress of 60 MPa, as compared to a standard switch with dimensions of 280x100x0.8 um. The variation of k over -50 to +90°C is ±30% and ±100% compared to ambient temperature for the miniature and standard switched capacitors, respectively.

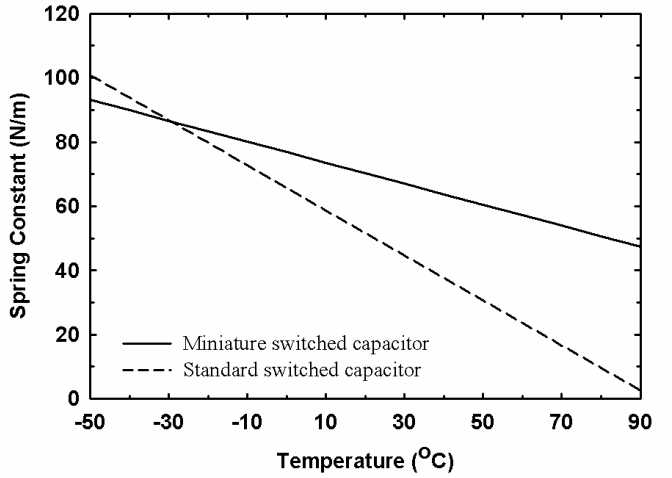

Fig. 2. Spring constant variations as a function of temperature for a miniature and a standard switched capacitor.

TABLE I
SWITCHED CAPACITOR DIMENSIONS (μm)

	Miniature switched capacitor	Standard switched capacitor
L_b	21	280
w_b	8	100
t_b	0.34	0.8
g_0	0.24	2
t_{diel}	0.16	0.2
W	8	100
G	9	100

The measured pull-down voltage is 23-25 V. Using (2), where $A=w_b \times W$, and the dimensions in Table I, the spring constant k is calculated to be 72 N/m which is in good agreement with the value obtained using (1) and σ=60 MPa. In (2), the dielectric thickness and fringing fields ($C_{ff}=0.12C_{pp}$) have been taken into account since the air gap is only 2× that of the dielectric thickness.

$$V_p = \sqrt{\frac{2kg_0\left(\frac{2g_0}{3}+\frac{t_{diel}}{\varepsilon_{rdiel}}\right)^2}{3A\varepsilon_0(1+0.12)}} \quad (2)$$

The effective mass m of the gold beam is 440 pg. Knowing k and m the mechanical resonant frequency f_0 of the beam is determined by $2\pi f_0 = \sqrt{k/m}$ and is 2 MHz. f_0 is 10-40× higher than standard RF MEMS switches or switched-capacitors and results in a much faster switching speed. With an actuation voltage of $1.25\times V_p$, the simulated switching speed is 250 ns for Au switches and 110 ns for Al switches (calculated with Q=1).

A major advantage of the miniature design is the pull-up force per unit contact area with the dielectric layer. As is well known, the predominant failure mechanism of capacitive switches is charging in the dielectric layer, and the miniature switches have 270 kN/m^2 of pull-up force as compared to a standard switched capacitor (or RF MEMS switch) with a pull-up force of only 9 kN/m^2 (see Table II). Our analysis, based on the work of Reid [4], indicates that the dielectric can charge to > 10^{12}/cm^2 and the miniature switch will still pull-up to its initial position. Therefore, it is expected that the miniature switched capacitor will be much more reliable than the standard RF MEMS capacitive switch.

TABLE II
SWITCHED CAPACITOR MECHANICAL PROPERTIES

	Miniature switched capacitor	Standard switched capacitor
Spring constant k, k_1, k_2 *	70, 48, 22 (N/m)	51, 3, 48 (N/m)
Effective mass Au, Al	440, 60 (pg)	172, 24 (ng)
f_0 Au; Al	2, 5.1 (MHz)	80, 240 (kHz)
Mechanical Q Au, Al **	0.5, 0.2	0.2, 0.1
Pull-down voltage	25 (V)	35 (V)
Switching time ($1.25V_p$) Au, Al ***	250, 110 (ns)	9, 3 (μs)
Pull-up force	17 (μN)	90 (μN)
Pull-up force per unit contact area	270 (kPa)	9 (kPa)

* k is calculated using σ=60 MPa
** can be increased to Q=1 using holes in the beam
*** Calculated with Q=1

III. FABRICATION

The MEM capacitors are fabricated on a 300 μm-thick high resistivity silicon substrate (> 2 kΩ-cm) on which a 5000 Å of SiO_2 is deposited using a PECVD machine. The first metal layer is a 100Å/1900Å of Ti/Au evaporated and etched to form the coplanar waveguide. Next, a 1600 Å thick dielectric layer (SiN) is deposited (PECVD), and the PMMA sacrificial layer is spin-coated (2400 Å) and patterned using a RIE. Then, the SiN dielectric layer is etched and the second metal layer deposited using a sputtered coater (Ti/Au/Ti 50Å/3300Å /50Å). This layer is selectively electroplated up to 1.5 μm in

order to obtain stiff anchorage and to reduce RF losses of the CPW line. Finally, the second metal layer is etched, the beams are released and the sample is dried in a CO_2 critical point drier.

Notice that the beam thickness is comparable to the center conductor thickness it is then critical to use a fabrication which results in very small step in the sacrificial layer in order to obtain beams with uniform thickness. Therefore, the SiN dielectric layer is not etched and covers entirely the CPW line from the ground to the center conductor (see Fig. 1). Fig. 3 shows a released gold bridge with uniform thickness, good planarity, and excellent step coverage.

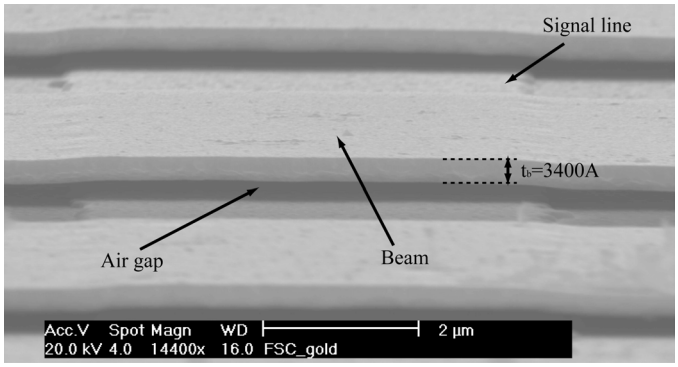

Fig. 3. SEM picture of the cross section of a miniature switched capacitor.

The structure is designed such that the residual stress has a limited effect on the mechanical properties, and the most important fabrication parameter is the thickness of the deposited bridge. This result in a more reliable fabrication process since the thickness is easy to control compared to the stress. Still, particular care should be taken to the different lithography steps concerning alignment and over etching.

(a)

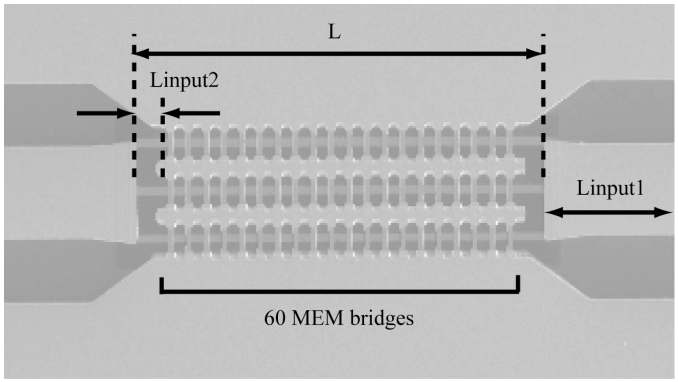

(b)

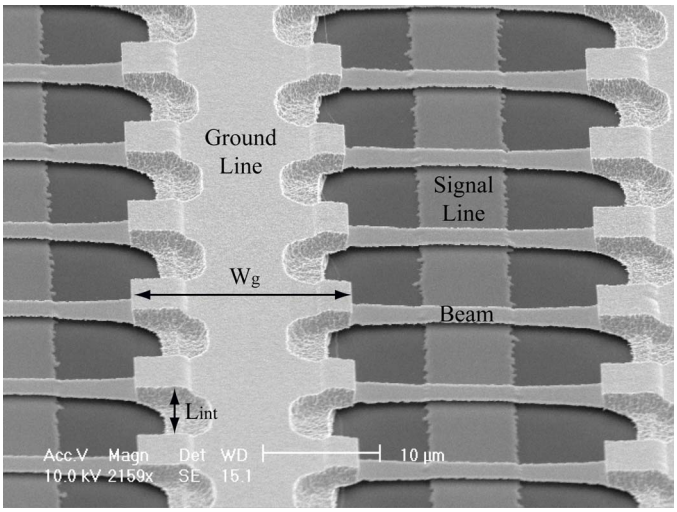

Fig. 4. SEM pictures of an array of miniature switched capacitor with 60 bridges (a), zoom view (b). The zoomed view is rotated 90° compared to the top view.

IV. MEASUREMENTS

The capacitance value in the up and down-state positions was determined by fitting a model to the measured S-parameters. A single capacitor has a very small capacitance which does not lead to accurate fitting at 2-20 GHz, and therefore, the measurements are performed on array of 60 bridges (3x20) as seen in Fig. 4. The measured S-parameters are shown in Fig. 5, and the electrical equivalent circuits are presented in Fig. 6 and Table III.

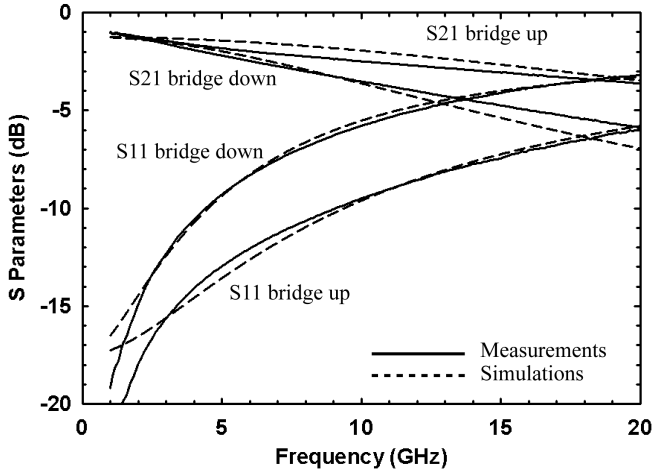

Fig. 5. Measured and modeled results for the array of switched capacitors in the up and in the down state.

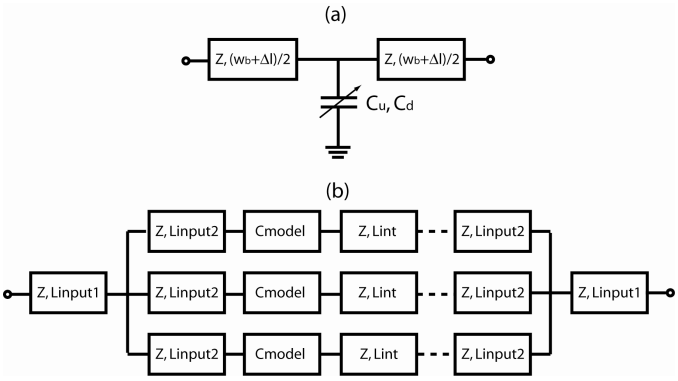

Fig. 6. Electrical equivalent model (Cmodel) of a single bridge (a), and the equivalent model of the 60 MEMS switched capacitor array (b).

Fig. 5 shows good agreement between measured and modeled results. The capacitance of a single bridge in the up-state C_u is 2.4 fF and includes C_{pp} (2.2 fF) and C_f (0.2 fF). The down-state capacitance C_d is 6.8 fF, and is limited by the roughness of the dielectric. This results in a capacitance ratio of 2.8. The measured capacitance of the entire array is 340 fF and 650 fF in the up and down-state positions, respectively, and is not 60× that of the single switch due to the inductive nature of the connecting t-lines between the individual switched capacitors.

TABLE III
CAPACITOR ARRAY DIMENSIONS (μm)

L	Length of the thin first metal layer	350
L_{int}	Distance between to bridges	9
W_g	Width of the Ground line	19
L_{input1}	Length of the input (line1)	250
L_{input2}	Length of the input (line2)	30

The quality factor of the switched capacitor array (60 bridges) is found using the electrical equivalent circuit. When the bridges are in the up-state position, (Cu=340 fF, X=-j91Ω at 5 GHz), the quality factor is 20 at 5 GHz. When the bridges are actuated (Cd=650 fF, X=-j49 Ω at 5 GHz), the quality factor is 10 at 5 GHz. The relatively low Q value is due to the narrow (8 μm) and thin (2000 Å) CPW t-lines between the bridges which result in a series resistance of around 5 Ω. In the near future, we will increase the narrow CPW-line width to 12 μm and its thickness to 4000 Å, and we believe that the Q will increase by a factor of 3. This will make the device ideal for switched-capacitor phase shifters and tunable networks.

Smaller devices with 20, 10 and 4 elements for Ku, Ka and W-Band applications are currently being measured. These are expected to have a much higher Q due to their smaller size.

V. CONCLUSION

This paper demonstrates the feasibility of very small RF MEMS switched capacitors. It proves that by decreasing the size, miniature switched capacitors with C_{on}/C_{off}=2.8 for a single bridge and C_{on}/C_{off}=1.9 for a 3×20 array, and excellent mechanical properties (high spring constant, high mechanical resonant frequency, very high speed actuation) can be fabricated. The structure is also less sensitive to temperature variations, vibrations or chocks than larger structures. We are currently in the process of measuring its switching speed, power handling, intermodulation properties, temperature characteristics and reliability.

ACKNOWLEDGEMENT

This work was supported by the USAF R L under contract # FA8718-04-C-0029.

REFERENCES

[1] G. M. Rebeiz, *RF MEMS Theory, Design, and Technology*, New York: J. Wiley & Sons, 2003.
[2] CoventoreWare[tm] version 2003, http://www.coventore.com
[3] J. Robert Reid, LaVern A. Starman, and Richard T. Webster, "RF Actuation of Capacitive MEMS Switches," *2003 IEEE MTT-S Int. Microwave Symp. Dig.*, vol. 3, pp. 1919-1922, June 2003.
[4] J. Robert Reid, "Simulation and measurement of dielectric charging in electrostatically actuated capacitive microwave switches," *Nanotech Int. Conf. Proc.*, vol. 1, pp. 250-253, 2002.

APPENDIX B
High-Power High-Reliability High-Q Switched RF MEMS Capacitors

Alex Grichener* Denis Mercier* and Gabriel M. Rebeiz†
*Department of Electrical Engineering and Computer Science, University of Michigan,
Ann Arbor MI, 48105
† Department of Electrical and Computer Engineering, University of California San Diego
La Jolla, CA 92093

***Abstract*— This paper presents an RF MEMS switched capacitor suitable for tunable filters and reconfigurable matching networks. The switched capacitor results in a capacitance ratio of 1.5−2 depending on the design, and a very high-Q ($>$ 225) at X to Ku-band frequencies. The switched-capacitor has been tested at 1 W of RF power at 8 GHz for $>$ 11 billion cycles under hot-switched conditions and a uni-polar actuation voltage of 0−50 V, with virtually no change in the C-V curve. The measured switching and release time is 8 μs. The main reason for this reliability performance is the absense of all dielectric layers in the RF MEMS capacitor.**

***Index Terms*— RF MEMS, tunable capacitors, reliability, tunable filters, reconfigurable network**

I. Introduction

RF MEMS switches are now quite mature with several excellent candidates having achieved $>$ 20 billion switching cycles (Radant MEMS, Raytheon, MIT-Lincoln Laboratories, University of Michigan, etc.) [1], and research has recently shifted towards the development of high-Q analog varactors or switched-capacitors for reconfigurable circuits. Notable developments in this field is the work of Dussopt et al. on the two-level switched-capacitors [2], Peroulis et al. on the extended analog varactor [3], B-Kassem at el. on an extended range analog varactor with tuning stops [4], Niemenen et al. on the temperature stable switched-capacitor [5], Muldavin et al. on the multi-bit switched-capacitor [6], Reid et al. on a 4-state digital variable capacitor [7], and Blondy et al. on a dielectric-less fixed-fixed beam switched capacitor [8]. This paper expands on the work of [7] which is based on a cantilever approach. The cantilever design results in high-temperature stability and the air-air (dielectric-less) design results in high-reliability operation. The design is shown to be very repeatable and with excellent performance.

II. Structure

The top view and cross section of the capacitive switch are presented in Fig. 1. The structure is cantilever-based with an air gap in both the up- and down-state positions. When a voltage is applied between the cantilever and the bottom electrode, the cantilever moves down until the dimples make contact with the landing pads which are electrically isolated from the electrode.

Electro-mechanical simulations of the structure above were performed using Coventorware. The results show an up-state capacitance of 85 fF, a down-state capacitance of 155 fF (capacitance ratio of 1.82), and a pull-in voltage of 37 V.

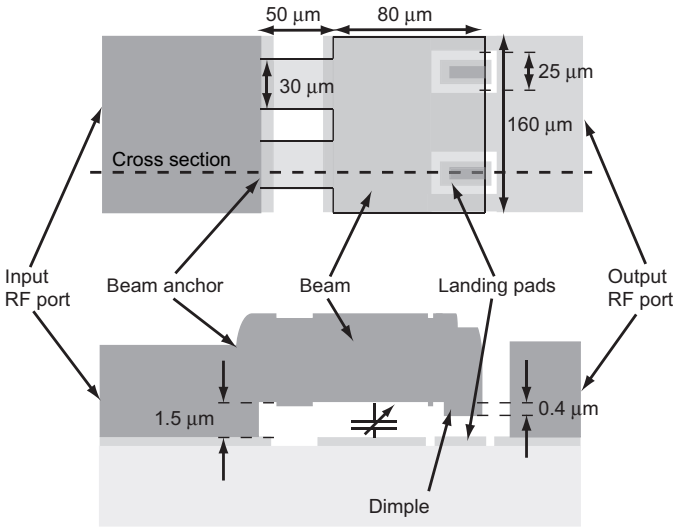

Fig. 1. Top view (top) and cross section (bottom) of switched capacitor.

III. Fabrication

The switches are fabricated on a 500 μm-thick glass substrate, and are implemented in a CPW line. First, the bottom metal layer consisting of Ti/Au (200 Å/5000 Å) is evaporated and patterned to form the bottom electrodes. Next, a 1.5 μm thick SiO_2 layer is deposited with PECVD as the sacrificial layer and patterned with RIE. The SiO_2 is then etched again with RIE to a depth of 0.4 μm at the dimple locations. Next, a second metal layer consisting of Ti/Au/Ti (200 Å/1000 Å/150 Å) is sputtered and selectively electroplated (5 μm) to form the cantilevers. Finally, the second metal is etched, the cantilevers are released in BHF, and the sample is dried in a CO_2 critical point dryer.

Two of the switch configurations that were fabricated are shown in Figures 2, and 3. The first device is a 1-port capacitive switch, and the second device is a 2-port capacitive switch in a series configuration. As the pictures show, each switch is attached to a short section of CPW line (about 160 μm) at the input port and at the output port (if it is a 2-port configuration).

IV. Measurements

A 1-port capacitive switch implemented in a CPW line, such as the one shown in Figure 2, was measured from 0.5 to 40 GHz in the up- and down-state positions. The actuation voltage was 35 V. The dimensions of this particular switch

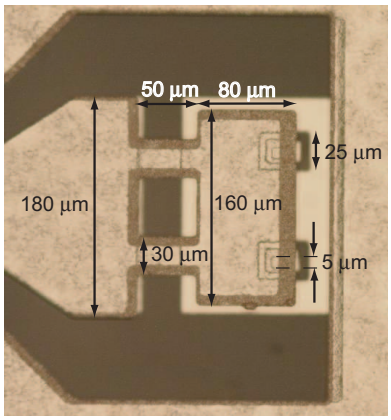

Fig. 2. Optical picture of a 1-port switched capacitor.

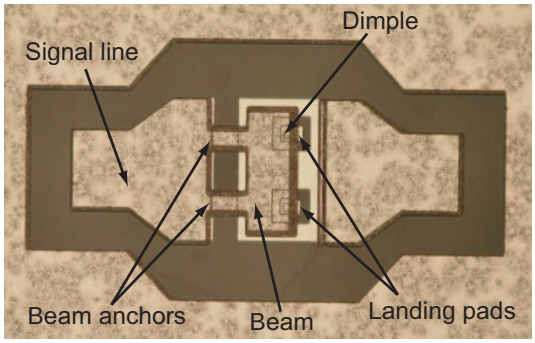

Fig. 3. Optical picture of a 2-port switched capacitor.

are exactly those shown in Figure 1. The up- and down-capacitance were extracted by fitting the simulated S_{11} of the equivalent model shown in Figure 4, to the measured S_{11}. Note that most of the inductance in the model physically comes from the two relatively thin arms connecting the anchors to the moving cantilever. Figure 5 shows the measured and simulated S_{11} of the switch in both states. The extracted capacitance ratio is 1.90.

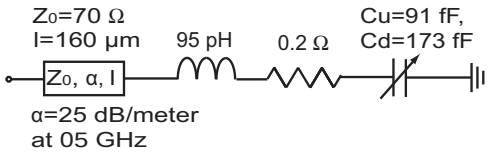

Fig. 4. Equivalent circuit model for a 1-port switched capacitor.

The formula for the quality factor of a series capacitor is simply:

$$Q = \frac{Imag(Z_{in})}{Real(Z_{in})} \quad (1)$$

where Z_{in} is the impedance of the switch and can be calculated from the measured S_{11}. However, the S_{11} measurement includes a bit of CPW transmission line (as seen in the equivalent model in Figure 4). For the final quality factor calculation, the purely reactive component of the line has been subtracted from $Imag(Z_{in})$. Whereas $Real(Z_{in})$ includes both the loss

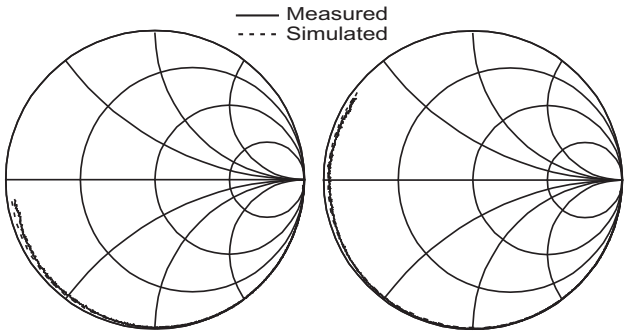

Fig. 5. Measured and simulated S_{11} of a 1-port switched capacitor in the up-state (left) and in the down-state (right).

of the switch and the loss of the line (since it is very hard to separate the two), thus giving a fairly conservative estimate of the quality factor. The resulting quality factor and reactance of the switch are shown in Table 1 for three different frequency points.

Table 1. De-embedded reactance and quality factor vs. frequency for a 1-port switched capacitor.

Frequency (GHz)	Up State (C_u=91 fF)		Down State (C_d=173 fF)	
	Reactance (Ohms)	Quality Factor	Reactance (Ohms)	Quality Factor
10	-169j	450	-86j	350
15	-108j	400	-52j	225
20	-76j	225	-34j	90

The measured Q is very high due to the thick gold cantilever and the wide bottom electrode. As is well known, the thickness of standard fixed-fixed varactors is about 0.5-1.5 μm (and not 5 μm as in this case) which has limited their Q to about 100-200 at 10-30 GHz. It must be stated that the Q is determined from S_{11} measurements and this does not yield an accurate result for Q $>$ 100. Still, the results are consistent in that the extracted Q falls with frequency as 1/f and also falls with capacitance as 1/C (as expected).

Figure 6 shows the extracted capacitance versus voltage curve for the 1-port capacitive switch. The measured pull-down voltage is 31 V and is 6 V lower than the simulated pull-down voltage. The extracted spring constant of the cantilever beam is 115 N/m.

The effective mass of the cantilever is 1.2 μg. Knowing k and m, the mechanical resonant frequency f_0 of the cantilever is determined by $2\pi f_0 = \sqrt{k/m}$ and is 50 KHz. Assuming a cantilever with a relatively small damping coefficient ($Q_m > 1$), the calculated switching time is given by [1]:

$$t_s \simeq 3.67 \frac{V_p}{V_s 2\pi f_0} \quad (2)$$

where V_p is the pull-down voltage and V_s is the actuation voltage. For a pull-down voltage of 31 V and an actuation voltage of 35 V the switching time is 10 μs.

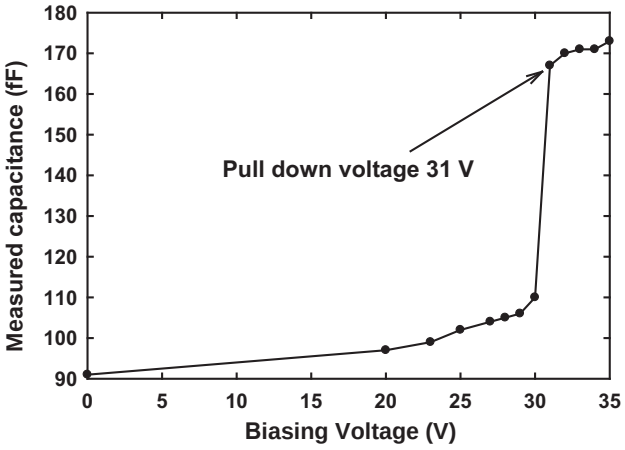

Fig. 6. Measured capacitance vs. voltage curve of a 1-port switched capacitor.

A 2-port capacitive switch, such as the one shown in Figure 3, was measured from 2 to 18 GHz, with an actuation voltage of 50 V. The switch dimensions are as shown in Figure 1 except the length of the cantilever was decreased from 80 μm to 70 μm and the width of the cutout for the landing pad was increased from 25 μm to 30 μm. The network analyzer internal bias-T did not allow a voltage higher than 40 V, and prevented us from measuring this device up to 40 GHz in the down-state position. The simulated S-parameters of the equivalent circuit model shown in Figure 7 are plotted versus the measured S-parameters in the up-state and in the down-state in Figure 8. The extracted capacitance ratio is 1.51.

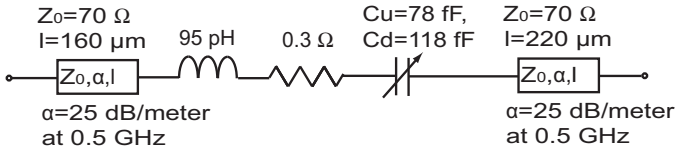

Fig. 7. Equivalent circuit model for a 2-port switched capacitor.

Table 2 lists the extracted capacitances for the two different kinds of fabricated switches, as well as their operating down-state voltage (this voltage was always chosen to be higher than the switch's pull-down voltage). The measured up- and down-state capacitance of the 1-port switch agree fairly well with the simulated values from section II. Also, the up-state capacitance is directly proportional to the cantilever-to-electrode face-to-face area, as expected.

However, the results show that the capacitance ratio of the 2-port switch is significantly lower than that of the 1-port switch. This may be due to differences in dimple heights due to fabrication errors, and some upward curling of the cantilever beams due to a stress gradient in the 5 μm thick gold beams.

V. Switching Speed and Reliability

The test setup for measuring the switching speed of a 2-port device is shown in Figure 9. A square unipolar voltage waveform is used to actuate the device. The reflected power

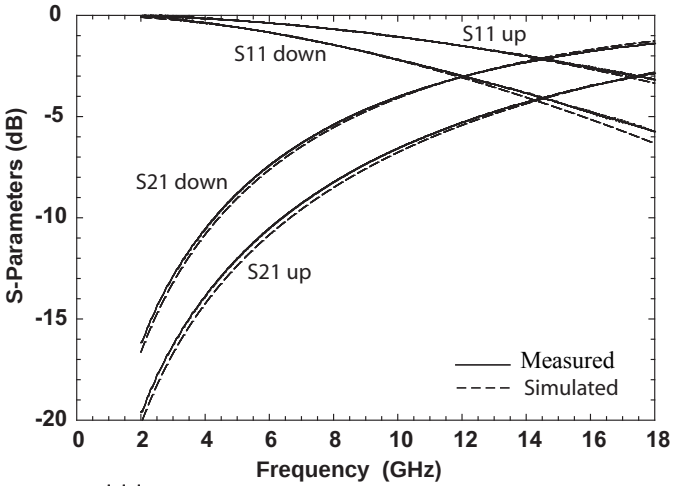

Fig. 8. Measured and simulated S-parameters of a 2-port switched capacitor in the up-state and in the down-state.

Table 2. Summary of extracted up- and down-state capacitance for the two fabricated switched capacitors.

Switch type	Face-to-face area (μm^2)	C_{up} (fF) per beam	C_{down} (fF) per beam	Ratio	Operating Voltage
1-port	12,200	91	173	1.90	35
2-port	10,450	78	118	1.51	50

is blocked by the 20 dB isolator and does not affect the measurement. The output RF power is measured with a diode detector.

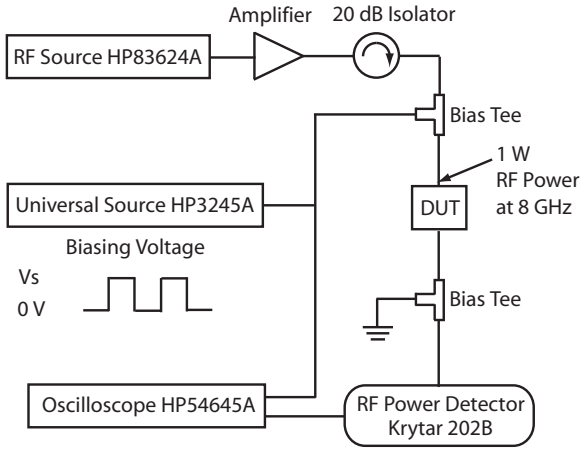

Fig. 9. Switching speed and reliability measurement test setup.

The switching speed of a 2-port capacitive switch, such as the one shown in Figure 3, was measured with this test setup. The switch was actuated at a rate of 10 KHz using a 0-35 V unipolar voltage and injected with 1 W of RF power at 8 GHz. Both the actuation voltage and the output voltage of the diode detector are plotted in Figure 10 during the up-to-down and down-to-up switch transitions. The plots show that the switching speed of this device is 8 μs which agrees with the calculated value from the previous section.

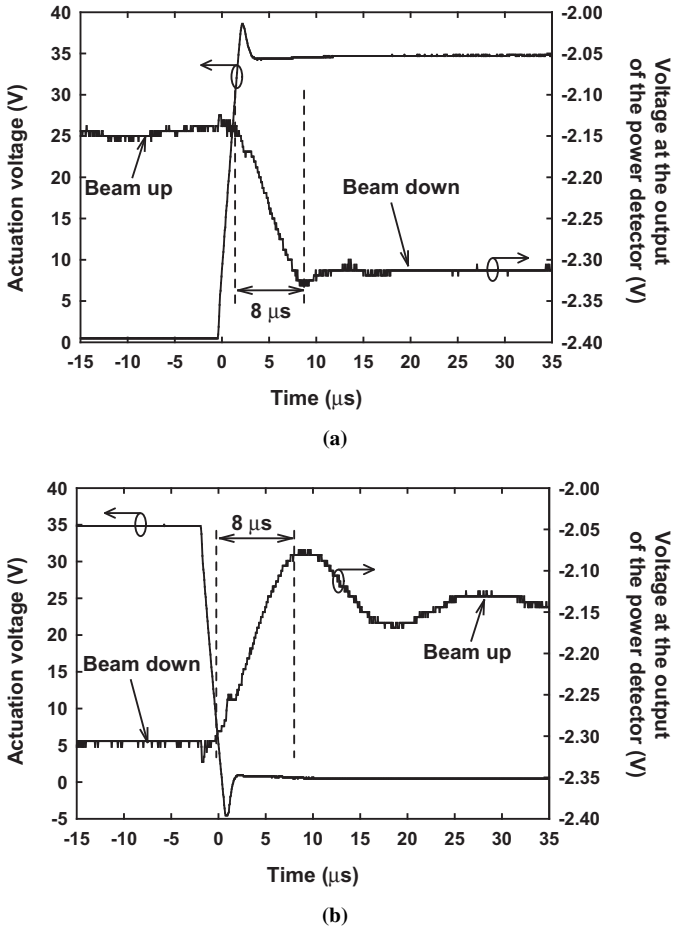

Fig. 10. Actuation voltage and detected power level vs. time for up-to-down (a) and down-to-up (b) capacitive switch transitions.

The 2-port switch went through reliability testing in the test setup depicted in Figure 9. The device was hot switched with 10 KHz, 0-50 V square waveform and with 1 W of RF power at 8 GHz (X_{up}=-255j at this frequency). The actuating square waveform and the detected output power were monitored on an oscilloscope. The device switched for over 11 billion cycles ($>$ 12 days of continuous switching) with no failure. The reliability testing was ceased because the test setup could not be reserved for a longer period of time.

Figure 11 shows the extracted capacitance versus voltage curve for the 2-port capacitive switch before and after reliability testing. The capacitance ratio has remained 1.51. Measurements indicate that the S-parameters have also remained nearly the same.

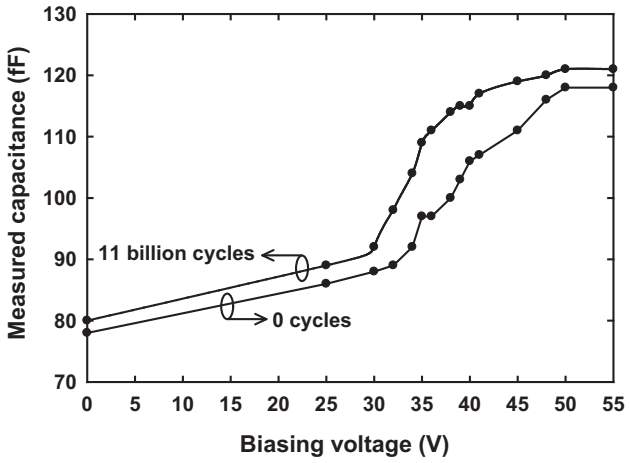

Fig. 11. Measured capacitance vs. voltage curve of a 2-port switched capacitor before and after reliability testing.

VI. Conclusion

A dielectric-less RF MEMS switched capacitor has been designed, fabricated and demonstrated. A capacitance ratio of 1.9 has been achieved for a switch implemented in a 1-port configuration. The switch shows a pull-down voltage of 31 V, and a switching speed of 8 μs. The thick gold cantilever and wide bottom electrode structure results in a Q $>$ 225 at X to Ku-band frequencies. High reliability was also demonstrated when the device was hot switched with 1 W of RF power at 8 GHz for $>$ 11 billion cycles with no failure and with little change in the C-V curve.

Acknowledgment

This work was supported by US-AFRL under contract FA8718-04-C-0029.

References

[1] G. M. Rebeiz, *RF MEMS Theory, Design, and Technology.* John Wiely and Sons, 2003.

[2] L. Dussopt, G. M. Rebeiz, "An X- to ku-band 3-bit digital MEMS varactor," *IEEE Microwave and Wireless Components Letters* vol. 13, issue 9, pp. 361-363, September 2003.

[3] D. Peroulis, Y. Lu, L. P. B. Katehi, "Highly reliable analog MEMS varactors," *2004 IEEE MTT-S Int. Microwave Symp. Dig.,* vol. 2, pp. 869-872, June 2004.

[4] M. Bakri-Kassem, R. R. Mansour, "An improved design for parallel plate MEMS variable capacitors," *2004 IEEE MTT-S Int. Microwave Symp. Dig.,* vol. 2, pp. 865-868, June 2004.

[5] H. Nieminen, V. Ermolov, S. Silanto, K. Nybergh, T. Ryhanen, "Design of a temperature-stable RF MEM capacitor," *Microelectromechanical Systems, Journal* vol. 13, issue 5, pp. 705-714, October 2004.

[6] J. Muldavin, C. Bozler, S. Rabe, C. Keast, "Large tuning range analog and multi-bit MEMS varactors," *2004 IEEE MTT-S Int. Microwave Symp. Dig.,* vol. 3, pp. 1919-1922, June 2004.

[7] J. R. Reid, L. A. Starman, R. T. Webster, "4-State digital variable capacitors," Proc. of Eurosensors XVIII, pp. 405-406, September 2004.

[8] P. Blondy, A. Crunteanu, C. Champeaux, A. Catherinot, P. Tristant, O. Vendier, J. L. Cazaux, L. Marchand, "Dielectric less capacitive MEMS switches," *2004 IEEE MTT-S Int. Microwave Symp. Dig.,* vol. 2, pp. 573-576, June 2004.

APPENDIX C
Low Loss 5.15-5.70 GHz RF MEMS Switchable Filter for Wireless LAN Applications

Sang-June Park, *Student Member, IEEE,* Kok-Yan Lee, *Member, IEEE,* and Gabriel M. Rebeiz, *Fellow, IEEE*

***Abstract*— Low loss 3.6 GHz fixed and 5.15 GHz-5.70 GHz RF MEMS switchable filters were designed and fabricated on quartz substrates. Detailed design equations for the capacitively-loaded coupled open-loop $\lambda/2$ resonators are given and the realization of the tunable filter using these equations is discussed. The use of capacitively-loaded coupled open-loop $\lambda/2$ resonators made it possible to realize the fixed and switchable filters with unloaded Q of around 150 resulting in a -1.4 dB insertion loss. The measured -1 dB bandwidth for the 3.6 GHz fixed and 5.15 GHz-5.70 GHz switchable filters were 4% and 5%, respectively. To our knowledge, this represents the lowest loss planar tunable filter to-date in the 4-6 GHz frequency range.**

***Index Terms*— RF MEMS, coupled open-loop resonators, capacitive loading, tunable filter, switchable filter.**

I. Introduction

TUNABLE filters are essential components for reconfigurable front-ends since they allow the use of a single component as opposed to a switched-filter bank, thereby reducing the system size and complexity. However, since they are placed between the antenna and the low-noise amplifier, they must exhibit very low loss and high linearity, especially in todays crowded RF environments. The tuning devices are solid-state varactor diodes or a p-i-n switch [1]- [3], ferroelectric varactors [4]- [5], or RF MEMS-based varactors or switched-capacitor banks. Notably, RF MEMS devices have been shown to have very high Q at RF to mm-wave frequencies (Q $>$ 200) and generate very low distortion levels (IM2 and IM3 components) [6]. Several notable examples of RF MEMS tunable filters are found in [7]- [15]. A close examination of the RF MEMS tunable filters in [7]- [15] shows overall resonator tunable Q values in the range of 40-60, which result in large insertion losses for 3-5% 2 and 3-pole filters, and therefore, it is imperative that the tunable Q be increased to $>$ 200 if possible.

A tunable Q $>$ 200 is not an easy feat using planar resonators. One needs to start with both a resonator Q and a tuning device Q $>$ 200, and special attention needs to be placed on any leakage due to resistive bias lines and radiation loss which can significantly reduce the Q. Also, the filter poles need to be accurately modeled for 3-5% designs, and any deviation from the correct values can seriously degrade the input impedance in the passband response. Entesari et al. achieved a 5$\pm$0.5% tunable filter covering 6-10 GHz and with an excellent match (S_{11} $<$ -16 dB), but the tunable Q was 40-50 over the 6-10 GHz range [11].

This paper presents a 5% 2-pole tunable 5.15/5.70 GHz filter based on an RF MEMS switched capacitor and with a tunable resonator Q $\geq$ 150, which is about a 3$\times$ improvement over previous designs. This is achieved using microstrip-based high-Q resonators in a shielded cavity, accurate electromagnetic simulation and design, and low-loss bias lines. Also, a comprehensive design methodology for the loaded ring resonators is introduced. The frequency selection is chosen to demonstrate its use for a WLAN system, but it is evident from this work that the same filter topology can be applied anywhere in the 1-40 GHz range. The measured response agrees very well with simulations, and shows that high-Q planar tunable filters can be achieved with RF MEMS devices.

II. Design

Hong et. al [16] showed how to extract the coupling and resonance frequency for the coupled open-loop structure presented in this paper using computer simulations. This method is very efficient for designing fixed frequency filters but for tunable filters, full analytic solutions need to be developed due to the introduction of tuning elements. The open-loop resonator with a loading varactor was also suggested by Makimoto et. al [17] (Fig. 1) but in that paper, only the analytical expression for a single capacitively-loaded resonator was given. The resonance frequency of a single *uncoupled* capacitively-loaded resonator is different from that of *coupled* capacitively-loaded resonators, and as the center frequency of the filter is varied by controlling the tuning elements, all of the filter parameters change. Therefore, to keep track of the tunable filter responses properly, analytical equations need to be developed.

A. Calculating Admittance Matrix of the Coupled Resonators

The *uncoupled* input admittance of the capacitively-loaded ring resonator (Fig. 1) can be found using:

$$Y_{in} = \frac{(-jY_1 \cot\phi_1 + j\omega C_L)^2 - (jY_1 \csc\phi_1 - j\omega C_L)^2}{-jY_1 \cot\phi_1 + j\omega C_L} \quad (1)$$

The above relation is easily determined by calculating the two-port network of Fig. 1b and open circuiting one of the ports.

This work was supported by US-AFRL under contract number FA8718-04-C-0029, Jack Ebel and Eric Marsh, contract monitors.

Sang-June Park is with the Radiation Laboratory, Department of Electrical Engineering and Computer Science, University of Michigan (e-mail: sangjp@umich.edu).

Gabriel M. Rebeiz is with the Department of Electrical and Computer Engineering, University of California, San Diego (email: rebeiz@ece.ucsd.edu).

Kok-Yan Lee is with the DSO Singapore on assignment at UM/UCSD (email: leeky@comcast.net).

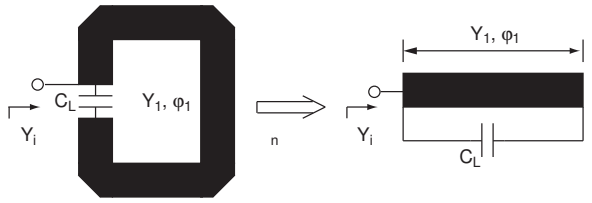

Fig. 1. Electrical circuit model of the resonator.

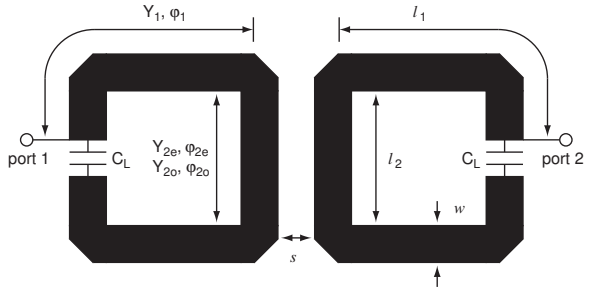

Fig. 2. Electrical circuit model of the coupled-resonator filter with 2 ports.

Calculating the admittance network of the coupled resonators in Fig. 2 requires more steps. The even-odd mode self admittances, Y_{ts_e} and Y_{ts_o} and mutual admittances, Y_{tm_e} and Y_{tm_o} of the coupled resonators are:

$$Y_{ts\_e} = \frac{A_e}{B_e} + j\omega C_L, \quad Y_{ts\_o} = \frac{A_o}{B_o} + j\omega C_L \tag{2}$$

$$Y_{tm\_e} = -\frac{1}{B_e} - j\omega C_L, \quad Y_{tm\_o} = -\frac{1}{B_o} - j\omega C_L \tag{3}$$

where

$$A_e = \cos 2\phi_1 \cos\phi_{2e} - \frac{1}{2}\left(\frac{Y_{2e}}{Y_1} + \frac{Y_1}{Y_{2e}}\right)\sin 2\phi_1 \sin\phi_{2e} \tag{4}$$

$$B_e = \frac{j\cos^2\phi_1}{Y_{2e}} - \frac{jY_{2e}\sin^2\phi_1 \sin\phi_{2e}}{Y_1^2} + \frac{j\sin 2\phi_1 \cos\phi_{2e}}{Y_1} \tag{5}$$

$$A_o = \cos 2\phi_1 \cos\phi_{2o} - \frac{1}{2}\left(\frac{Y_{2o}}{Y_1} + \frac{Y_1}{Y_{2o}}\right)\sin 2\phi_1 \sin\phi_{2o} \tag{6}$$

$$B_o = \frac{j\cos^2\phi_1}{Y_{2o}} - \frac{jY_{2o}\sin^2\phi_1 \sin\phi_{2o}}{Y_1^2} + \frac{j\sin 2\phi_1 \cos\phi_{2o}}{Y_1} \tag{7}$$

The even-odd mode input admittances of the coupled resonators are then:

$$Y_{in\_e} = \frac{Y_{ts\_e}^2 - Y_{tm\_e}^2}{Y_{ts\_e}}, \quad Y_{in\_o} = \frac{Y_{ts\_o}^2 - Y_{tm\_o}^2}{Y_{ts\_o}} \tag{8}$$

The overall admittance matrix of the capacitively-loaded coupled resonators is then [18]:

$$Y = \begin{bmatrix} \frac{Y_{in\_e} + Y_{in\_o}}{2} & \frac{Y_{in\_e} - Y_{in\_o}}{2} \\ \frac{Y_{in\_e} - Y_{in\_o}}{2} & \frac{Y_{in\_e} + Y_{in\_o}}{2} \end{bmatrix} \tag{9}$$

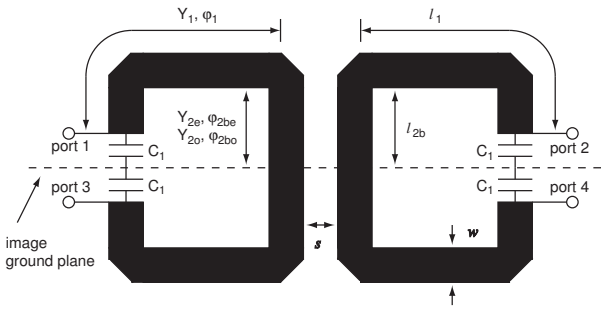

Fig. 3. Electrical circuit model of the coupled resonator filter with 4 ports.

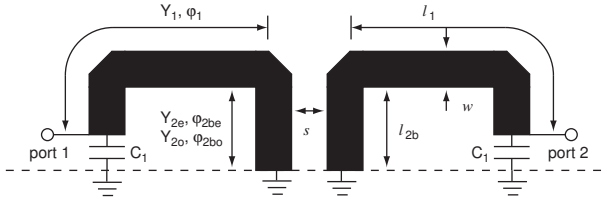

Fig. 4. Electrical circuit model of the tunable filter with half-plane symmetry.

B. Design of the Tunable Filter Using Analytical Methods

1) Calculating the loading capacitor, C_L, and even-odd mode admittances, Y_{2e} and Y_{2o}: The admittance network above (Fig. 2) needs to satisfy two conditions to be a filter network. The network should have the resonance frequency and the coupling coefficient of the desired filter. The two conditions are:

$$Im[Y_{11}(\omega_0)] = 0, \quad \frac{Im[Y_{12}(\omega_0)]}{b} = k_{12} \tag{10}$$

where

$$b = \frac{\omega_0}{2}\frac{\partial Im[Y_{11}(\omega_0)]}{\partial\omega}, \quad k_{12} = \frac{\Delta}{\sqrt{g_1 g_2}} \tag{11}$$

Solving (10) and (11) gives the loading capacitance, C_L, and even-odd admittances, Y_{2e} and Y_{2o}. As can be seen in the above equation, the slope parameter, b, is a function of the loading capacitance, C_L. Because Y_{2e}, Y_{2o} and C_L are coupled in (10) and (11), it is not easy to find the explicit solutions.

The difficulty in the above design equations can be bypassed if the symmetric property of the filter network is considered. As can be seen in Fig. 3, there is a virtual ground plane in the center plane of the filter. Because of this plane, it is possible to take into account only the upper or lower half of the filter network.

Fig. 4 shows the equivalent upper half of the filter network. This filter network is a capacitively-loaded $\lambda/4$ coupled structure and it is possible to decouple C_1 from the slope parameter, b. Therefore, explicit expressions for C_1, Y_{2e}, and Y_{2o} can be found as follows:

a) The even-odd mode input admittances of the filter network in Fig. 4 are:

$$Y_{re} = \frac{-jY_1 Y_{2e}\cot\phi_{2be} + jY_1^2\tan\phi_1}{Y_1 + Y_{2e}\cot\phi_{2be}\tan\phi_1} \tag{12}$$

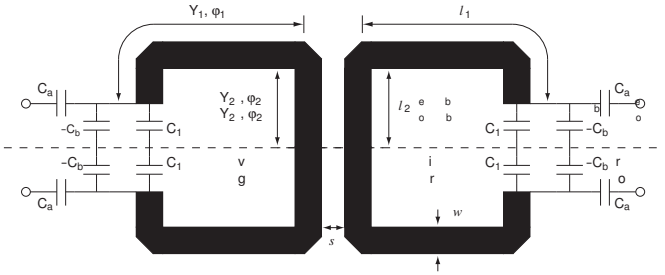

Fig. 5. The balanced filter with the capacitive J-inverter section.

$$Y_{ro} = \frac{-jY_1Y_{2o}\cot\phi_{2bo} + jY_1^2\tan\phi_1}{Y_1 + Y_{2o}\cot\phi_{2bo}\tan\phi_1} \tag{13}$$

b) The overall admittance matrix of this filter network is:

$$Y_r = \begin{bmatrix} \frac{Y_{re}+Y_{r_o}}{2} + j\omega C_1 & \frac{Y_{re}-Y_{ro}}{2} \\ \frac{Y_{re}-Y_{ro}}{2} & \frac{Y_{re}+Y_{ro}}{2} + j\omega C_1 \end{bmatrix} \tag{14}$$

c) The resonance condition, $Im[Y_{r11}(\omega_0)] = 0$, gives:

$$C_1 = -Im\left[\frac{Y_{re}(\omega_0) + Y_{ro}(\omega_0)}{2\omega_0}\right] \tag{15}$$

d) From the above result, b is then calculated using:

$$b = Im\left[\frac{\omega_0}{4}\frac{\partial\{Y_{re}(\omega_0)+Y_{ro}(\omega_0)\}}{\partial\omega} - \frac{Y_{re}(\omega_0)+Y_{ro}(\omega_0)}{4}\right] \tag{16}$$

e) Once b is determined, the even-odd admittances, Y_{2e}, Y_{2o}, are found explicitly by:

$$\frac{Im[Y_{re}(\omega_0) - Y_{ro}(\omega_0)]}{Im\left[\frac{\omega_0}{2}\frac{\partial\{Y_{re}(\omega_0)+Y_{ro}(\omega_0)\}}{\partial\omega} - \frac{Y_{re}(\omega_0)+Y_{ro}(\omega_0)}{2}\right]} = \frac{\Delta}{\sqrt{g_1 g_2}} \tag{17}$$

which utilizes the property of the coupling coefficient:

$$k_{12} = \frac{Im[Y_{r12}(\omega_0)]}{b} = \frac{\Delta}{\sqrt{g_1 g_2}}. \tag{18}$$

After determining the even-odd admittances, Y_{2e} and Y_{2o}, the loading capacitance, C_1, can be calculated using (15).

The original filter network in Fig. 3 has the same filter response as Fig. 4 due to the symmetry. Therefore, the even-odd admittances, Y_{2e} and Y_{2o}, are the same as (12) and (13) and the loading capacitor, C_L, is $C_1/2$.

2) Realizing external coupling, Q_{ext}: For a tunable filter, the tapping or transformer coupling methods are not appropriate when a wide tuning range is required. As is well known, the slope parameter, b, is dependent on the frequency, and any change in b results in a poor impedance match. Capacitive coupling is a good candidate for realizing wide frequency tuning because by changing the capacitance values, the slope parameter variation can be compensated completely. A frequency scaling network (J-$inverter$) consisting of a series positive capacitance with a shunt negative capacitance is the most popular solution [19].

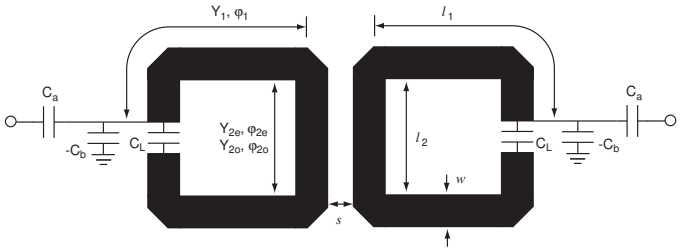

Fig. 6. The single-ended filter with the capacitive J-inverter section.

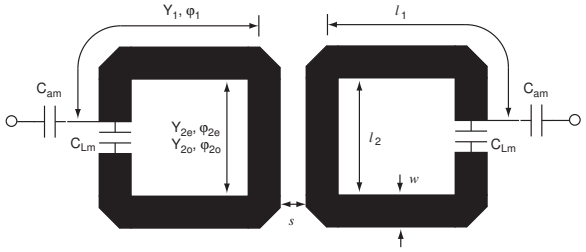

Fig. 7. The single-ended filter with modified input and loading capacitors.

For the $balanced$-type filter in Fig. 5, it is easy to realize the external coupling capacitance network because the negative capacitance value, -C_b, of the J-$inverter$ section can be absorbed by the loading capacitance, C_1, by virtue of the image ground plane presented in the symmetry plane. The modified loading capacitor, C_{Lb}, and input capacitor, C_a, are given by:

$$C_{Lb} = \frac{C_1 - C_b}{2}, \quad C_a = \frac{J_{01}}{\omega_0\sqrt{1-(J_{01}/Y_0)^2}} \tag{19}$$

where

$$J_{01} = \sqrt{\frac{Y_0 b\Delta}{g_0 g_1}}, \quad C_b = \frac{J_{01}^2}{\omega_0^2 C_a^2} \tag{20}$$

The single-ended filter needs special attention when the J-$inverter$ section is realized by series/shunt capacitances (Fig. 6). J_{01} in (20) needs to be calculated using b in (11) and the negative capacitance, -C_b, cannot be absorbed in the loading capacitor, C_L, because the symmetry plane does not exist in the structure any more. Therefore, instead of using the capacitive J-$inverter$ section, the modified input capacitance C_{am}, and modified loading capacitor, C_{Lm}, in Fig. 7 can be directly found by setting two conditions: Let Z_j and Z_m be the impedance matrices of the filter networks in Fig. 6 and Fig. 7, respectively. The reactance value of Z_{m11} and its slope parameter, x_m, should be the same as the reactance value of Z_{j11} and its slope parameter, x_j, around the designed frequency, ω_0. The two conditions are:

$$Im[Z_{m11}(\omega_0)] = Im[Z_{j11}(\omega_0)], \quad x_m(\omega_0) = x_j(\omega_0) \tag{21}$$

where

$$x_m = \frac{\omega}{2}\frac{\partial Im\,[Z_{m11}]}{\partial\omega}, \quad x_j = \frac{\omega}{2}\frac{\partial Im\,[Z_{j11}]}{\partial\omega} \tag{22}$$

Equation (21) can be solved in terms of C_{am} and C_{Lm} because the impedance Z_{j11} and reactance slope parameter, x_j, can be obtained with known capacitance values, C_a and C_b in Fig. 6.

Assuming the admittance, Y_{Lm11}, as Y_{11}, in (9) with C_L replaced by C_{Lm}, the impedance, Z_{m11}, is:

$$Z_{m11} = Z_{Lmr} + \frac{1}{j\omega C_{am}} \tag{23}$$

where

$$Z_{Lmr} = \frac{Y_{Lm11}}{Y_{Lm11}^2 - Y_{Lm12}^2} \tag{24}$$

From the first equality in (21), C_{am} is expressed as:

$$C_{am} = \frac{1}{\omega_0} Im\left[\frac{1}{Z_{j11}(\omega_0) - Z_{Lmr}(\omega_0)}\right] \tag{25}$$

The reactance slope parameter, x_m, of the modified filter network in Fig. 7 is:

$$x_m(\omega_0) = \frac{\omega_0}{2}\frac{\partial Im\left[Z_{Lmr}(\omega_0)\right]}{\partial\omega} + \frac{1}{2\omega_0 C_{am}} \tag{26}$$

By using (25), x_m can be a function of only C_{Lm}, and is given by:

$$x_m(\omega_0) = Im\left[\frac{\omega_0}{2}\frac{\partial Z_{Lmr}(\omega_0)}{\partial\omega} + \frac{1}{Z_{j11}(\omega_0) - Z_{Lmr}(\omega_0)}\right] \tag{27}$$

Using the above equation, the second equality in (21) gives C_{Lm} and C_{am}, can be then found using (25)

C. Design of the Fixed 3.6 GHz Single-Ended Filter

A 0.1 dB ripple filter with a center frequency of 3.6 GHz and a 4.2% (150 MHz) bandwidth was designed using the equations in the previous section. The initial design parameters are, w = 1 mm, l_1 = 4.6 mm, l_2 = 1.5 mm on a 0.508 mm quartz substrate.

From (17), the calculated even-odd mode impedances, Z_{2e} and Z_{2o}, are 59.9 Ω and 43.9 Ω, respectively, and the corresponding gap, s is 0.40 mm. Once the even-odd admittances of the coupled section are found, the loading capacitance, C_1, is given by (15). The calculated value of C_1 = 0.84 pF, and this corresponds to a loading capacitor, C_L = 0.42 pF.

Using the dimensions above, the susceptance values of Y_{11} and Y_{12} in (9) are plotted in Fig. 8. As can be seen, this filter network resonates at 3.6 GHz and has two transmission zeroes, one at 2.1 GHz and the other at 6 GHz. The locations of the two zeroes will change slightly after the J-inverter coupling sections are added in the filter.

The modified loading capacitor, C_{Lm}, is found using (21) and (27). In this case, the variable, Δx_{norm} was defined and plotted in Fig. 9. The variable Δx_{norm} is:

$$\Delta x_{norm} = \frac{x_m(\omega_0) - x_j(\omega_0)}{x_j(\omega_0)} \tag{28}$$

From Fig. 9, C_{Lm} values of 0.35 pF and 0.50 pF are found, but the 0.50 pF is neglected because it results in a negative value of C_{am}. The modified input capacitance, C_{am}, is then given by (25) and is 0.40 pF.

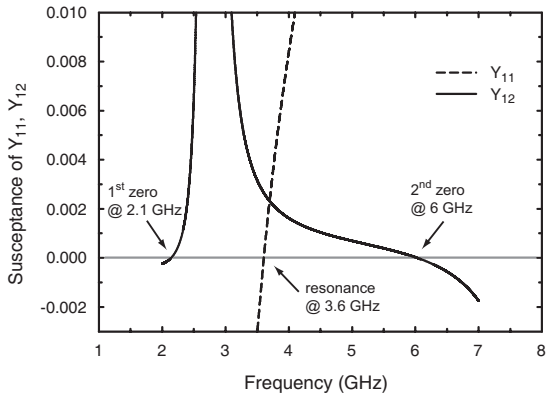

Fig. 8. Susceptance values of 3.6 GHz filter.

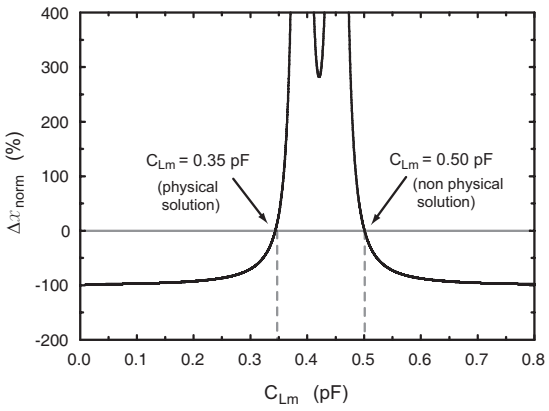

Fig. 9. Δx_{norm} in terms of C_{Lm}.

D. Implementation of the Fixed 3.6 GHz Single-Ended Filter

A full-wave simulation of the coupled resonator structure in Fig. 3 (without capacitors) is performed using SONNET [20] and the 4-port Y-parameters are extracted. The 4-port full-wave Y-matrix is:

$$Y^{4p} = \begin{bmatrix} Y_{11}^{4p} & Y_{12}^{4p} & Y_{13}^{4p} & Y_{14}^{4p} \\ Y_{12}^{4p} & Y_{11}^{4p} & Y_{14}^{4p} & Y_{13}^{4p} \\ Y_{13}^{4p} & Y_{14}^{4p} & Y_{11}^{4p} & Y_{12}^{4p} \\ Y_{14}^{4p} & Y_{13}^{4p} & Y_{12}^{4p} & Y_{11}^{4p} \end{bmatrix} \tag{29}$$

The 2-port Y-parameters of the coupled resonator structure in Fig. 4 (with capacitors) are found using the symmetric property of the 4-port full-wave network. The 2-port full-wave Y-matrix is:

$$Y^{2p} = \begin{bmatrix} Y_{11}^{4p} - Y_{13}^{4p} + j\omega C_1 & Y_{12}^{4p} - Y_{14}^{4p} \\ Y_{12}^{4p} - Y_{14}^{4p} & Y_{11}^{4p} - Y_{13}^{4p} + j\omega C_1 \end{bmatrix} \tag{30}$$

and C_1 is calculated by satisfying $Y_{11}^{2p} = 0$:

$$C_1 = -Im\left[\frac{Y_{11}^{4p}(\omega_0) - Y_{13}^{4p}(\omega_0)}{\omega_0}\right] \tag{31}$$

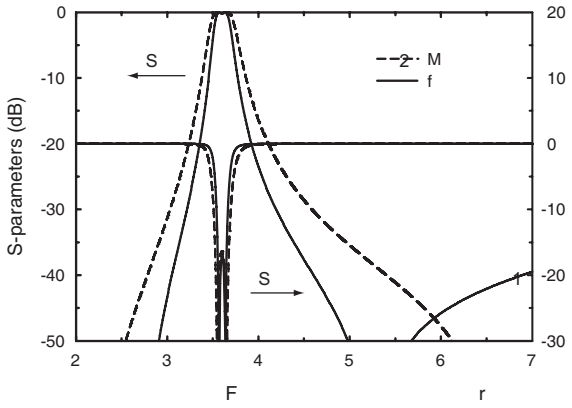

Fig. 10. Matlab and full-wave simulation of the fixed 3.6 GHz filter

The 2-port Y-parameters of the filter in Fig. 2 are then found by inserting C_L between ports 1 and 3 and ports 2 and 4 in (29), and open-circuiting ports 3 and 4. The 2-port full-wave Y-matrix is:

$$Y_f = \begin{bmatrix} Y_{f11} & Y_{f12} \\ Y_{f12} & Y_{f11} \end{bmatrix} \tag{32}$$

and the Y_{f11} and Y_{f12} are:

$$Y_{f11} = Y_{b11}^{4p} - \frac{Y_{b11}^{4p}[(Y_{b13}^{4p})^2 + (Y_{14}^{4p})^2] - 2Y_{12}^{4p}Y_{b13}^{4p}Y_{14}^{4p}}{(Y_{b11}^{4p})^2 - (Y_{12}^{4p})^2} \tag{33}$$

$$Y_{f12} = Y_{12}^{4p} - \frac{2Y_{b11}^{4p}Y_{b13}^{4p}Y_{14}^{4p} - Y_{12}^{4p}[(Y_{b13}^{4p})^2 + (Y_{14}^{4p})^2]}{(Y_{b11}^{4p})^2 - (Y_{12}^{4p})^2} \tag{34}$$

where

$$Y_{b11}^{4p} = Y_{11}^{4p} + j\omega C_L, \quad Y_{b13}^{4p} = Y_{13}^{4p} - j\omega C_L \tag{35}$$

C_{Lm} and C_{am} are then calculated using the procedures in (22)-(29), and are 0.47 pF and 0.36 pF, respectively. The filter responses from the MATLAB calculation [21] and the full-wave simulation are compared in Fig. 10. The full-wave simulation results in a larger C_{Lm} than the MATLAB calculation, and this is due to the mitered corners. The mittered corners result in a shorter l_1 and this in turn results in a larger capacitance value than the analytical solution (MATLAB). Also, the full-wave simulation shows a smaller bandwidth (3.4%) than the MATLAB simulation in Fig. 10. In the full-wave structure, the resonators are bent inward twice and because of this bending, there is coupling between the l_1 section and the l_2 section. This coupling reduces the coupling in section l_2 and results in a smaller bandwidth. This also explains why the transmission zeros are at different frequencies for the analytical calculation and the full-wave simulations.

When the capacitance values C_{am} and C_{Lm} are physically realized, one needs to consider that although (30) assumes point ports at the open ends of the resonators, a finite area is required to physically implement C_{am} and C_{Lm}. Both C_{am} and C_{Lm} are 0.40 mm long and 0.80 mm wide. The point port

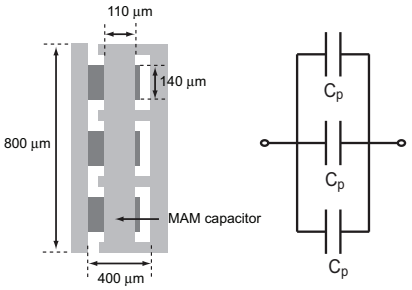

Fig. 11. Realization of the capacitance values, C_{Lm} and C_{am} (C_p=153 fF, C_{Lm}=C_{am}=3C_p = 460 fF).

TABLE I
COMPARISON OF SIMULATED CAPACITANCE VALUES FOR THE FIXED 3.6 GHZ FILTER (CAPACITANCES ARE IN fF)

	$MATLAB$ (calculation)	$SONNET$ (point ports)	$SONNET$ (physical ports)
C_{Lm}	350	470	460
C_{am}	400	360	460

assumption is good for C_{Lm} because C_{Lm} fits in the 0.4 mm gap between the open ends of the resonators. However, the point port assumption does not produce the correct value of C_{am} because of the 0.8 mm phyical width of C_{am}. Therefore, in the full-wave simulation including the physical capacitors, the capacitance values are modified to compensate for the shifted input/output ports and the junction effect of the input capacitor. The capacitance values resulting from the MATLAB calculations, the SONNET simulation assuming "point" ports, and the SONNET simulation with physical capacitors are summarized in Table I. The physical C_{Lm} and C_{am} are shown in Fig. 11 and are composed of 3 metal-air-metal capacitors, each of value C_p = 153 fF (C_{Lm} = C_{am} = 460 fF).

E. Implementation of the Tunable 5.15-5.70 GHz RF MEMS Filter

The same dimensions as the 3.6 GHz filter are used to design a tunable 5.15 GHz to 5.70 GHz filter, and the loading capacitances are calculated using (15). Fig. 12 shows the

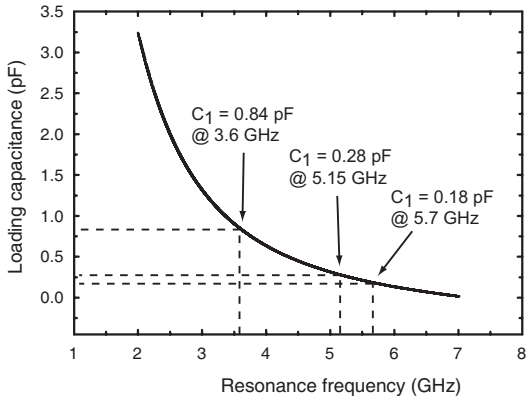

Fig. 12. Loading capacitor, C_1, in terms of resonance frequency.

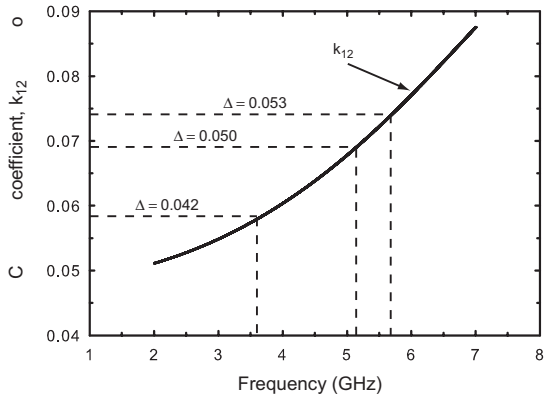

Fig. 13. Simulated coupling coefficient of the 2-pole filter at 3-6 GHz.

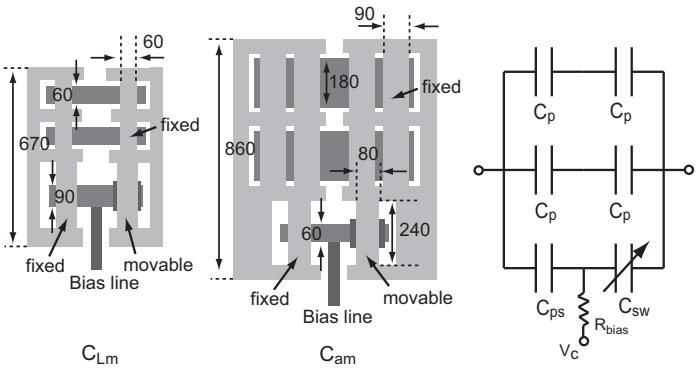

Fig. 14. Realization of 1-bit capacitance switch network (All dimensions in μm. For C_p and C_{ps} values, see Table II).

variation of loading capacitance, C_1, as a function of the resonance frequency, f_0. At 5.15 GHz and 5.70 GHz, the loading capacitance values are 0.28 pF and 0.18 pF, respectively.

In designing a tunable filter, it is important to keep track of the coupling coefficient variation in terms of resonance frequency. Using the relation in (17), the coupling coefficient, k_{12} is plotted as a function of f_0 (Fig. 13). At 3.6 GHz, the coupling coefficient value corresponds to 4.2% fractional bandwidth. At 5.15 GHz and 5.70 GHz, the coupling coefficient, k_{12}, corresponds to fractional bandwidths of 5.0% and 5.3% respectively.

The calculated (MATLAB) C_{Lm} and C_{am} for 5.15 GHz are 92 fF and 230 fF, respectively and the full-wave simulation results for the same C_{Lm} and C_{am} are 150 fF and 240 fF, respectively. At 5.70 GHz, the MATLAB calculations result in C_{Lm} and C_{am} values of 46 fF and 210 fF, respectively, while the full-wave simulation results are 94 fF and 210 fF, respectively. Again this is mainly due to the mitered corners which have a similar effect at 5.15-5.70 GHz.

To realize the changes in the loading and input capacitance values, the 1-bit switch circuit shown in Fig. 14 is proposed, and because of the MEMS fabrication issues, the dimension and aspect ratio of the capacitors are limited. The capacitance values for the switch network are summarized in Table II. In the C_{Lm} networks, there are lines that connect capacitors in series and C_{am} newtorks have 0.86 mm width. Therefore, in full-wave simulation including the capacitors, the capacitance

TABLE II

CAPACITANCE VALUES IN SWITCH NETWORK FOR THE 5.15 TO 5.70 GHZ SWITCHABLE FILTER (CAPACITANCES ARE IN fF)

	C_{ps}	C_p	$C_{sw}^{up}/C_{sw}^{down}$	$C_{total}^{up}/C_{total}^{down}$
C_{Lm}	90	45	95/1470	90/130
C_{am}	55	275	70/950	305/325

TABLE III

COMPARISON OF SIMULATED CAPACITANCE VALUES IN SWITCH NETWORK FOR THE 5.15 TO 5.70 GHZ SWITCHABLE FILTER (CAPACITANCES ARE IN fF)

$5.15/5.70\ GHz$

	$MATLAB$ (calculation)	$SONNET$ (point ports)	$SONNET$ (physical ports)
C_{Lm}	92/46	150/94	130/90
C_{am}	230/210	240/210	325/300

values were modified to compensate for the reactive effects of the lines and the shifted port of the capacitors. (Table III).

III. FABRICATION AND MEASUREMENTS

A. 3.6 GHz Fixed Filter

The filters are fabricated on a 0.508 mm quartz substrate (ϵ_r = 3.78 and tanδ = 0.0001) using a standard RF MEMS process developed at the University of Michigan [11], [22]. The resonators are electroplated to 3 μm thick using a low stress gold solution. For the 3.6 GHz filter, metal-air-metal (MAM) capacitors are used to realize the loading and input capacitors, C_{Lm} and C_{am}. The top electrode of the MAM

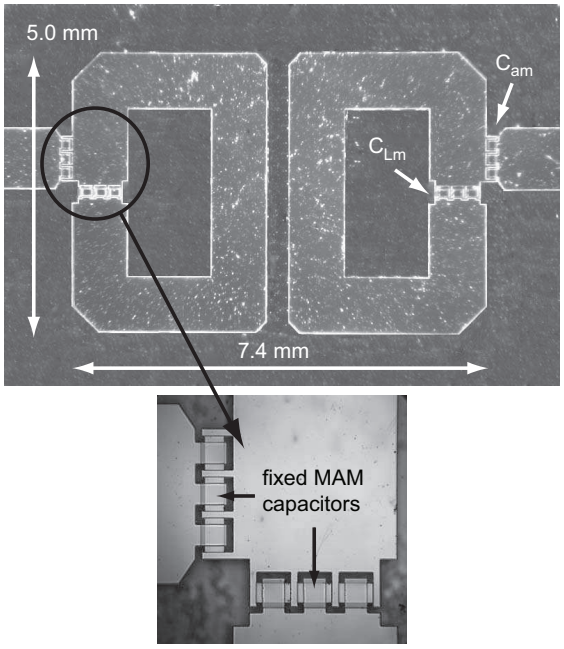

Fig. 15. Fabricated 3.6 GHz fixed filter on quartz substrate.

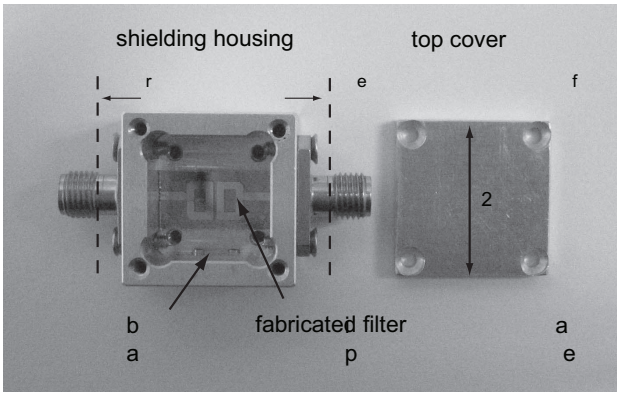

Fig. 16. The fabricated filter in the shielding housing (cover removed).

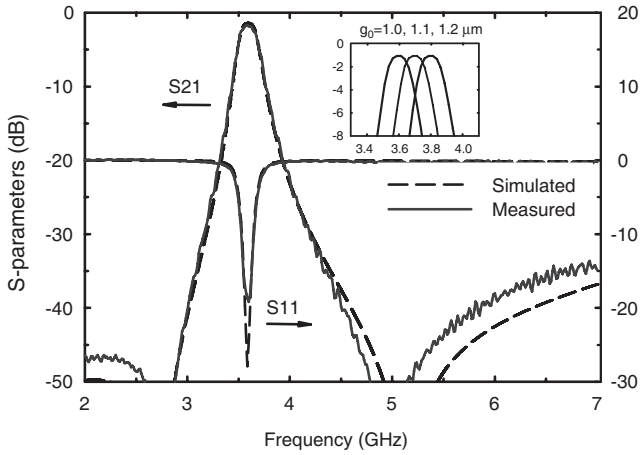

Fig. 17. Measurement vs. simulation of the fixed 3.6 GHz filter (g_0=1.0 μm).

capacitor is 3 μm thick. The bottom electrode is 0.6 μm thick and the air gap, g_0, is 1.1±0.1 μm.

The fabricated 3.6 GHz fixed filter and the measurement set up are shown in Figs. 15 and 16. The C_{Lm} and C_{am} consist of three MAM capacitors connected in parallel. The calibration is done using SOLT and is referenced to the RF connector. The measurement includes -0.1 dB loss due to the coax-microstrip transition of input ports. The measured and simulated results are plotted in Fig. 17, and are in excellent agreement. The measured and simulated insertion loss are -1.8 and -1.7 dB, respectively and the -1 dB bandwidth is 4.0% (144 MHz). The unloaded Q of capacitively loaded resonator was simulated (Q_u = 140) and measured (Q_u = 120) using the critical point method [23].

It is important to note that in Fig. 17, we have used g_0 as a fitting parameter in the simulated S-parameters. The reason is that we have a ± 0.1μm uncertainty on g_0 (1.1± 0.1 μm) and the final gap height is not known. A change of ± 0.1μm in g_0 results in a change of ±45 fF in C_{Lm} (or C_{am}) and a change of ±120 MHz in the filter response. In the future, and for precise frequency control, a small analog varactor or a mini-MEMS switch capacitor needs to be used [24].

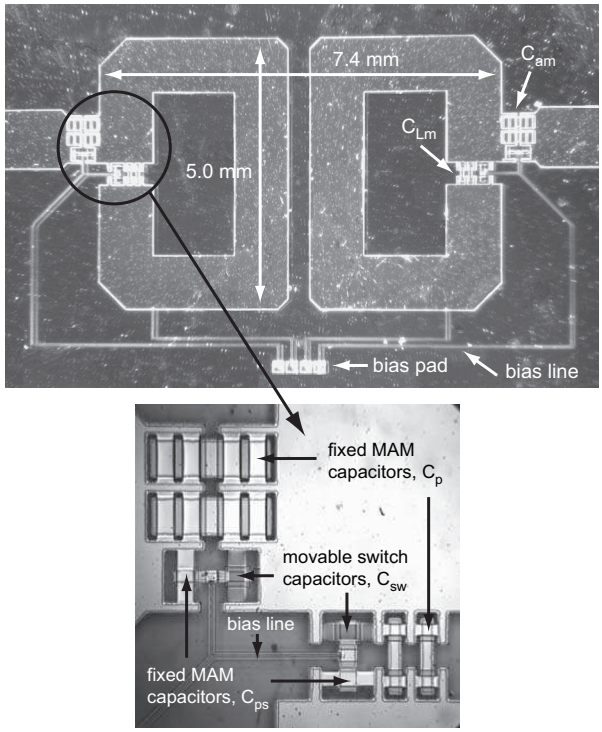

Fig. 18. Fabricated 5.15 to 5.70 GHz switchable filter on a quartz substrate.

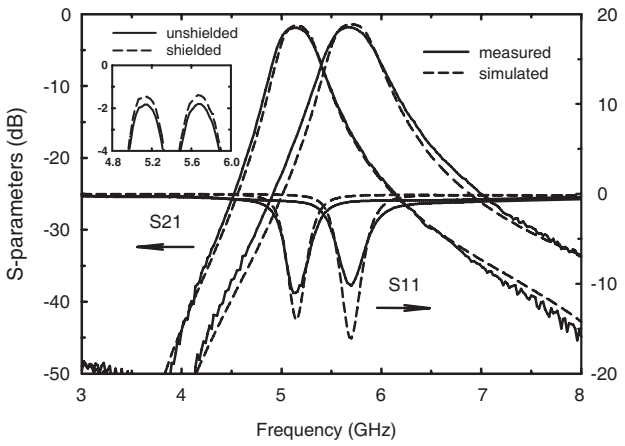

Fig. 19. Measurement vs. simulation of the 5.15 to 5.70 GHz tunable filter (g_0=1.1 μm).

B. 5.15 GHz-5.70 GHz RF MEMS Filter

The fixed MAM capacitors (C_{sp}, C_p) for the switchable filter have the same characteristics as the previous section. The switch capacitor, C_{sw} uses a 0.18 μm thick Si_3N_4 layer between the MEMS bridge and the bottom electrode. The 0.8 μm sputtered gold layer is suspended 1.1±0.1 μm above the pull-down electrode and the bias lines are fabricated using 0.08 μm-thick $SiCr$ with a resistivity of approximately 2 kΩ/□ and a line width of 20 μm. The bias line, if not well designed, can degrade filter performance by 1-2 dB [11]. However, in this case, the bias lines have virtually no effect on the filter performance due to the microstrip nature of the filter and the very low coupling to the 2 kΩ/□ lines. The measured pull-down voltage, V_p, is 25 V which corresponds to a spring

TABLE IV
MEASURED AND SIMULATED VALUES FOR THE 5.15 TO 5.7 GHZ SWITCHABLE FILTER

$Measured/Simulated$

	$f_0(GHz)$	$I.L.(dB)$	$BW(\%)$	Q
up-state	5.69/5.70	1.4/1.3	5.0/4.9 (285 MHz)	150/160
down-state	5.14/5.15	1.5/1.4	5.0/4.8 (257 MHz)	140/150

constant of 67 N/m for a gap of 1.1 μm, and a residual stress of 85 MPa. The mechanical resonance frequency, f_0, quality factor, Q_m and the switching time (V_a = 1.2V_p) of the switch are 120 kHz, 0.7, and 4-5 μs, respectively [25].

The fabricated 5.15-5.70 GHz tunable filter is shown in Fig. 18. It has two switchable capacitance networks at each resonator. The positive bias lines are connected to each switch (bottom electrode) and the DC ground bias lines are connected to the resonators. Fig.19 presents the measured and simulated frequency responses. The center frequencies of both the up and down-states shifted a little (15 MHz). The shift appears to be caused by slightly larger than predicted input capacitance. At 5.15 and 5.70 GHz the measured insertion loss of the filter is -1.8 dB and results in an unloaded Q of 120 (fitted to simulation). When the filters are completely shielded using a top cover, the insertion loss improves by 0.3 dB. Also, the transition loss (-0.1 dB) can be extracted from the measured loss. Therefore the actual loss of this filter is -1.5 to -1.4 dB corresponding to an unloaded Q of 140 to 150. The measured and simulated results are summarized in Table. IV.

IV. CONCLUSION

This paper presents a planar RF MEMS filter with a tunable resonator Q $\simeq$ 150. The filter is based on a capacitively-loaded open-loop resonators which result in a high resonator Q while still allowing for an excellent tuning response. The RF MEMS tunable filter results in a 5% bandwidth for a tuning range of 5.15$-$5.70 GHz with an insertion loss of only -1.4 to -1.5 dB. It is evident from this work that RF MEMS are an essential component for high-Q tunable filters. Future work includes improving the tunable resonator Q to $>$ 250 using suspended substrates and demonstration of this technique in the 10-40 GHz range.

REFERENCES

[1] Hunter, I. C., Rhodes, J. D., "Electronically Tunable Microwave Bandpass Filters," *IEEE Trans. Microwave Theory & Tech.*, vol. 30, no. 9, pp. 1354-1360, Sep. 1982.

[2] Brown, A. R., Rebeiz, G. M., "A Varactor-Tuned RF Filter," *IEEE Trans. Microwave Theory & Tech.*, vol. 48, no. 7, pp. 1157-1160, Jul. 2000.

[3] Lugo, C. Jr., Papapolymerou, J., "Electronic switchable bandpass filter using PIN diodes for wireless low cost sytem-on-a-package applications," *IEE Proc.-Microw. Antennas Propag.*, vol. 151, no. 6, pp. 497-502, Dec. 2004.

[4] Tombak, A., Maria, J.-P., Ayguavives, F., T., Jin, Zhang, Stauf, G. T., Kingon, A. I., Mortazawi, A., "Voltage-Controlled RF Filters Employing Thin-Film Barium-Strontium-Titanate Tunable Capacitors," *IEEE Trans. Microwave Theory & Tech.*, vol 51, no. 2, pp. 462-467, Feb. 2003.

[5] Nath, J., Ghosh, D., Maria, J.-P., Kingon, A. I., Fathelbab, W., Franzon, P. D., Steer, M. B., "An Electronically Tunable Microstrip Bandpass Filter Using Thin-Film Barium-Strontium-Titanate (BST) Varactors," *IEEE Trans. Microwave Theory & Tech.*, vol 53, no. 9, pp. 2707-2712, Sep. 2005.

[6] Dussopt, L., Rebeiz, G. M., "Intermodulation Distortion and Power Handling in RF MEMS Switches, Varators, and Tunable Filters," *IEEE Trans. Microwave Theory & Tech.*, vol 51, no. 4, pp. 1247-1256, Apr. 2003.

[7] Young, R.M., Adam, J.D., Vale, C.R., Braggins, T.T., Krishnaswamy, S.V., Milton, C.E., Bever, D.W., Chorosinski, L.G., Li-Shu Chen, Crockett, D.E., Freidhoff, C.B., Talisa, S.H., Capelle, E., Tranchini, R., Fende, J.R., Lorthioir, J.M., Tories, A.R., "Low-Loss Bandpass RF Filter Using MEMS Capacitance Switches to Achieve a One-Octave Tuning Range and Independently Variable Bandwidth," in *IEEE MTT-S Int. Microwave Symp. Dig.*, Philadelphia, PA, Jun. 2003, pp. 1781-1784

[8] Pothier, A., Orlianges, J.-C., Guizhen Zheng, Champeaux, C., Catherinot, A., Cros, D., Blondy, P., Papapolymerou, J., "Low-Loss 2-bit Tunable Bandpass Filters Using MEMS DC Contact Switches," *IEEE Trans. Microwave Theory & Tech.*, vol 53, no. 1, pp. 354-360, Jan. 2005.

[9] Pillans, B., Malczewski, A., Allison, R., Brank, J., "6-15 GHz RF MEMS tunable filters," in *IEEE MTT-S Int. Microwave Symp. Dig.*, Long Beach, CA, Jun. 2005, pp. 919-922

[10] Kim, J.-M., Lee, S., Park, J.-H., Kim, J.-M., Baek, C.-W.,Kwon, Y., Kim, Y.-K., "Digitally Frequency-Controllable Dual-Band WLAN Filters Using Micromachined Frequency-Tuning Elements," in *19th IEEE MEMS 2006 Conf.*, Istanbul, Turkey, Jan. 2006, pp. xxx-xxx.

[11] Entesari, K. and Rebeiz, G. M., "A differential 4-bit 6.5-10 GHz RF MEMS Tunable Filter," *IEEE Trans. Microwave Theory & Tech.*, vol. 53, no. 3, pp. 1103-1110, Mar. 2005.

[12] Entesari, K. and Rebeiz, G. M., "A 12-18 GHz Three-Pole RF MEMS Tunable Filter," *IEEE Trans. Microwave Theory & Tech.*, vol. 53, no. 8, pp. 2566-2571, Aug. 2005.

[13] Nordquist, C.D., Muyshondt, A., Pack, M.V., Finnegan, P.S., Dyck, C.W., Reines, I.C., Kraus, G.M., Plut, T.A., Sloan, G.R., Goldsmith, C.L., Sullivan, C.T., "An X-band to Ku-band RF MEMS switched coplanar strip filter," *IEEE Microw. Wireless Compon. Lett.*, vol. 14, no. 9, pp. 425-427, Sep. 2004.

[14] Lakshminarayanan, B., Weller, T., "Tunable bandpass filter using distributed MEMS transmission lines," in *IEEE MTT-S Int. Microwave Symp. Dig.*, Philadelphia, PA, Jun. 2003, pp. 1789-1792.

[15] Abbaspour-Tamijani, A., Dussopt, L., Rebeiz, G.M., "Miniature and tunable filters using MEMS capacitors," *IEEE Trans. Microwave Theory & Tech.*, vol. 51, no. 7, pp. 1878-1885, Aug. 2005.

[16] Hong, J.-S., Lancaster, M. J., "Couplings of Microstrip Square Open-Loop Resonators for Cross-Coupled Planar Filter," *IEEE Trans. Microwave Theory & Tech.*, vol. 44, no. 12, pp. 2099-2109, Dec. 1996.

[17] Makimoto, M., Sagawa, M., "Varactor Tuned Band Pass Filters Using Microstrip-Line Ring Resonators," in *IEEE MTT-S Int. Microwave Symp. Dig.*, Baltimore, MD, Jun. 1986, pp. 411-414.

[18] Park, S.-J., Van Caekenberghe, K., Rebeiz, G.M., "A Miniature 2.1-GHz Low Loss Microstrip Filter With Independent Electric and Magnetic Coupling," *IEEE Microw. Wireless Compon. Lett.*, vol. 14, no. 10, pp. 496-498, Oct. 2004.

[19] I. Hunter, *Theory and Design of Microwave Filters*, London, U.K.: The Institution of Electrical Engineers, 2001.

[20] SONNET 9.52, SONNET Software Inc., Syracuse, NY, USA.

[21] MATLAB 6.5, The MathWorks Inc., Natick, MA, USA.

[22] Hayden, J. S., Rebeiz, G. M., "Very low loss distributed X-band and Ka-band MEMS phase shifters using metal-air-metal capacitors," *IEEE Trans. Microwave Theory & Tech.*, vol. 51, no. 1, pp. 309-314, Jan. 2003.

[23] Sun, E.-Y., Chao, S.-H., "Unloaded Q Measurement-The Critical-Points Method," *IEEE Trans. Microwave Theory & Tech.*, vol. 43, no. 8, Aug. 1995, pp. 1983-1986.

[24] Mercier, D., Van Caekenberghe, K., Rebeiz, G.M., "Miniature RF MEMS switched capacitors," in *IEEE MTT-S Int. Microwave Symp. Dig.*, Long Beach, CA, Jun. 2005, pp. 745-748.

[25] G. M. Rebeiz, *RF MEMS Theory, Design, and Technology*, New York, USA: Wiley, 2003.